ELSEVIER

Earth and Planetary Science Letters 208 (2003) 235–252

EPSL

www.elsevier.com/locate/epsl

Paleomagnetic paleolatitude of Early Cretaceous Ontong Java Plateau basalts: implications for Pacific apparent and true polar wander

Peter Riisager [a,b,*], Stuart Hall [c], Maria Antretter [d], Xixi Zhao [b]

[a] *Danish Lithosphere Centre, Øster Voldgade 10, 1350 Copenhagen K, Denmark*
[b] *Earth Sciences Department, University of California at Santa Cruz, Santa Cruz, CA 95064, USA*
[c] *Department of Geosciences, University of Houston, Houston, TX 77204-5007, USA*
[d] *Institut für Geophysik, University of München, Theresienstrasse 41, 80333 Munich, Germany*

Received 11 November 2002; received in revised form 13 January 2003; accepted 14 January 2003

Abstract

We present paleomagnetic data from basaltic pillow and lava flows drilled at four Ocean Drilling Program (ODP) Leg 192 sites through the Early Cretaceous (~120 Ma) Ontong Java Plateau (OJP). Altogether 270 samples (out of 331) yielded well-defined characteristic remanent magnetization components all of which have negative inclinations, i.e. normal polarity. Dividing data into inclination groups we obtain 5, 7, 14 and 15 independent inclination estimates for the four sites. Statistical analysis suggests that paleosecular variation has been sufficiently sampled and site-mean inclinations therefore represent time-averaged fields. Of particular importance is the finding that all four site-mean inclinations are statistically indistinguishable, strongly supporting indirect seismic observation from the flat-lying sediments blanketing the OJP that the studied basalts have suffered little or no tectonic disturbance since their emplacement. Moreover, the corresponding paleomagnetic paleolatitudes agree excellently with paleomagnetic data from a previous ODP site (Site 807) drilled into the northern portion of the OJP. Two important conclusions can be drawn based on the presented dataset: (i) the Leg 192 combined mean inclination (Inc. = −41.4°, $N = 41$, $k = 66.0$, $\alpha_{95} = 2.6°$) is inconsistent with the Early Cretaceous part of the Pacific apparent polar wander path, indicating that previous paleomagnetic poles derived mainly from seamount magnetic anomaly modeling must be used with care; (ii) the Leg 192 paleomagnetic paleolatitude for the central OJP is ~20° north of the paleogeographic location calculated from Pacific hotspot tracks assuming the hotspots have remained fixed. The difference between paleomagnetic and hotspot calculated paleolatitudes cannot be explained by true polar wander estimates derived from other lithospheric plates and our results are therefore consistent with and extend recent paleomagnetic studies of younger hotspot features in the northern Pacific Ocean that suggest Late Cretaceous to Eocene motion of Pacific hotspots.

Keywords: Ocean Drilling Program Leg 192; Ontong Java Plateau; paleomagnetic paleolatitude; hotspots; Pacific apparent polar wander path; true polar wander

* Corresponding author. Fax: +45-33-11-08-78. *E-mail address:* peter@es.ucsc.edu (P. Riisager).

0012-821X/03/$ – see front matter © 2003 Elsevier Science B.V. All rights reserved.
doi:10.1016/S0012-821X(03)00046-3

1. Introduction

The Pacific apparent polar wander path (APWP) is pivotal for testing circum-Pacific plate reconstructions [1], fixity of hotspots [2], and the significance of true polar wander (TPW) estimates derived from other lithospheric plates [3–4]. Unfortunately, it is difficult to draw rigid conclusions based on the presently available Pacific APWP as different oceanic paleomagnetic datasets have yielded mutually inconsistent results, indicating that the reliability of some Pacific paleomagnetic poles may be uncertain.

In this paper we present a new Pacific paleomagnetic paleolatitude estimate from ~120 Ma ocean floor basalts obtained from the Ontong Java Plateau (OJP; Fig. 1). The estimate is based on direct paleomagnetic data from four independent drill sites, which allow us to discuss uncertainties, such as non-averaged paleosecular variation and/or tectonic disturbances, that are not easily detected at individual drill sites [5]. In the following we will compare our new ~120 Ma OJP paleomagnetic paleolatitude estimate with the Pacific APWP, and discuss the significance in relation to TPW, hotspot fixity, and Pacific plate reconstructions.

2. Geology and sampling

2.1. Formation and geological setting of the OJP

The OJP (Fig. 1) is the world's largest volcanic oceanic plateau with a surface area of 1.9×10^6 km^2 and an estimated volume of $4–5\times10^7$ km^3 [6]. Existing age constraints point to the formation of the OJP in a single geologically brief period around 120 Ma [7–10], making it the largest magmatic event on Earth during the last 200 Myr.

It is unclear whether the OJP was emplaced at a seafloor spreading center or away from active plate boundaries [11]. Almost all oceanic crust west and south of the plateau has been subducted and possible magnetic lineations as well as fracture zone fabric of sub-OJP ocean floor are subdued and thus cannot be interpreted unambiguously [12]. Irrespective of the original plate tectonic settings, anomalously hot lower mantle material must have been present to produce the enormous total partial melt volume [13] as well as the composition of the lavas [14]. The OJP formation is therefore best explained by the plume-head or plume-impact model (e.g. [15–16]) in which widespread basaltic flood eruptions occur as the inflated head of a rising new mantle plume approaches the base of the lithosphere. The OJP, however, lacks an obvious plume tail trace (hotspot track) and cannot be directly linked to any known hotspot source. The suggested formation above the initial plume head of the Louisville hotspot [15,17] is not supported by geochemical evidence [18] or plate reconstructions [12].

Two points of major importance for the paleomagnetic analysis are: (i) the M-series magnetic lineations in basins east and north of the plateau [19], documenting that since its formation the OJP has remained a coherent part of the Pacific plate and OJP paleomagnetic data can therefore be directly compared with other Pacific data; (ii) although post-emplacement deformation has taken place along the northern and southern margins of the plateau [12,17,20], the four Ocean Drilling Program (ODP) Leg 192 sites (Fig. 1) have suffered little or no tectonic disturbance since the time (~90 Ma) of the earliest visible sedimentary reflector [8]. Based on the paleomagnetic data we discuss possible tectonic disturbances below.

2.2. Sampling

A more than 1 km thick blanket of pelagic sediments covers most areas of the OJP and it is therefore difficult to sample the underlying volcanic rocks suitable for paleomagnetic paleolatitude studies. During the two previous scientific drill cruises to the OJP (Deep Sea Drilling Project Leg 30 and ODP Leg 130) basement material was recovered from only three drill sites, two of which did not recover enough for any comprehensive paleomagnetic study. Only at Site 807 (Fig. 1) was sufficient material recovered to average out secular variation [21]. We discuss Site 807 paleomagnetic data in more detail below.

The ODP Leg 192 cruise was specifically designed to retrieve basement material, and we

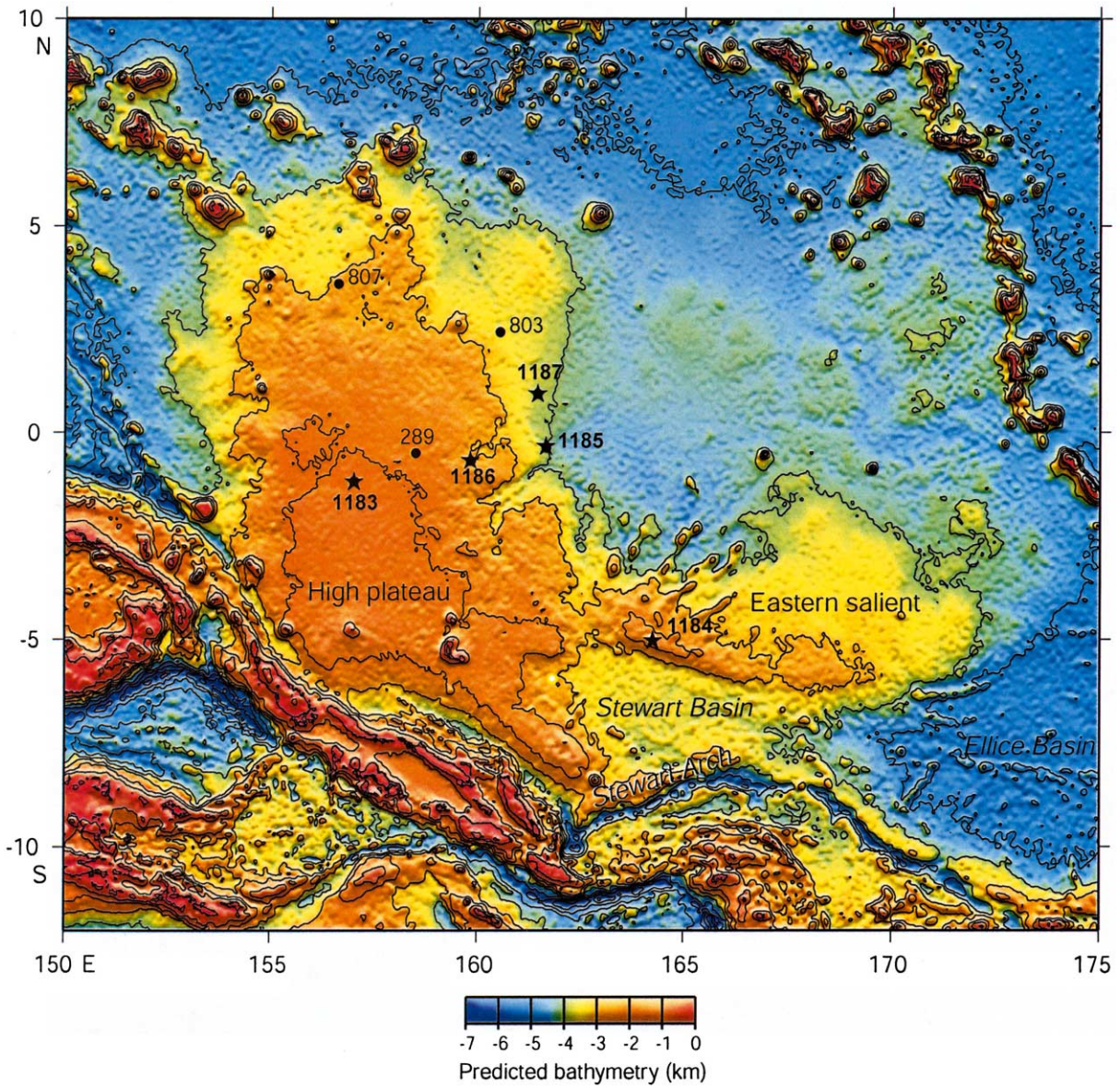

Fig. 1. Predicted bathymetry (after [48]) of the OJP showing the location of Leg 192 drill sites (stars). Filled circles indicate previous ODP and DSDP sites that reached basement; only Site 807 drilled a sufficiently long interval of basaltic lavas (148.7 m) to supply a time-averaged paleomagnetic inclination estimate.

therefore succeeded in coring significant amounts of ocean floor basalts at four out of five sites (Fig. 1). A majority of the igneous units were pillow basalts with only a few intervals of apparently more massive subaqueous lava flows. All rocks have been affected by low-temperature alteration processes in amounts similar to those found in normal seafloor basalts [8]. The paleomagnetic samples were obtained from pieces long enough to ensure that their up–down orientation was preserved during rotary coring. Samples were spaced at irregular intervals, with the object of collecting at least four to five samples from each igneous unit. From the altogether 518.7 m of basalts

Table 1
Inclinations of the ChRM component

Core	Section	Interval (cm)	Depth (mbsf)	Inclination (°)	Intensity (mA m^2/kg)	MAD (°)	Demag type	Inclination group
Site 1183								
54R	4	91–93	1131.58	Unstable			Th	
54R	5	36–38	1132.49	−54.7	0.64	1.4	AF	1
55R	1	48–50	1136.98	Unstable			AF	
55R	1	87–89	1137.37	−55.9	0.69	3.6	AF	1
55R	2	24–26	1137.99	−65.0	0.34	3.1	AF	1
55R	3	131–33	1140.45	−55.4	0.90	4.6	AF	1
56R	1	12–14	1146.22	Unstable			AF	
56R	1	94–96	1147.04	−30.9	1.28	2.4	AF	2
56R	2	8–10	1147.53	−47.9	1.43	3.4	AF	2
56R	3	20–22	1149.13	−33.5	2.35	0.9	AF	2
57R	1	131–33	1152.31	−38.8	1.20	1.6	AF	2
57R	2	43–45	1152.88	−46.4	1.58	3.1	AF	2
57R	3	6–8	1154.01	−45.9	0.64	2.5	AF	2
58R	1	121–123	1157.01	−36.1	1.07	2.9	AF	2
58R	2	29–31	1157.51	Unstable			Th	
58R	3	58–60	1159.19	−55.1	1.47	0.6	AF	2
59R	1	60–62	1161.20	−48.3	1.06	1.3	AF	2
59R	1	129–131	1161.89	−44.9	1.34	3.4	AF	2
59R	2	63–65	1162.68	Unstable			Th	
60R	1	136–38	1167.86	−58.2	1.10	1.3	AF	3
60R	2	9–11	1168.07	−51.0	1.12	1.6	AF	3
61R	1	76–78	1176.86	−48.5	0.89	1.4	AF	3
61R	1	134–36	1177.44	−59.4	0.95	5.3	AF	3
61R	2	38–40	1177.86	−37.9	0.94	2.4	AF	4
62R	1	63–65	1181.63	−42.0	1.98	3.9	AF	4
62R	2	61–63	1183.01	−43.5	1.51	3.1	AF	4
62R	3	30–32	1184.20	−44.1	2.97	3.1	AF	4
63R	1	45–47	1186.25	−47.2	0.67	2.0	AF	4
63R	1	94–96	1186.74	−42.9	2.59	3.1	AF	4
64R	1	41–43	1191.01	Unstable			Th	
64R	2	81–83	1192.81	−29.6	3.69	1.2	AF	5
65R	1	45–47	1195.85	Unstable			AF	
65R	1	100–102	1196.40	−38.2	1.46	3.0	AF	5
65R	2	63–65	1197.43	−46.9	1.08	2.8	AF	5
65R	3	28–30	1198.44	−37.1	1.85	3.6	AF	5
66R	1	24–26	1200.34	−36.0	2.11	9.2	AF	5
66R	1	132–134	1201.42	−32.4	0.55	5.5	AF	5
66R	2	26–28	1201.76	−54.7	0.68	1.3	AF	5
66R	3	12–14	1203.06	−34.9	1.19	4.0	AF	5
67R	1	2–4	12–.92 04	−23.5	3.88	2.7	AF	5
67R	1	23–25	1205.13	−41.0	1.65	2.5	AF	5
67R	1	92–94	1205.82	−32.3	1.77	1.7	Th	5
67R	2	7–9	1206.42	−30.9	1.49	4.8	AF	5
67R	2	99–101	1207.34	−42.0	0.73	1.3	AF	5
67R	3	72–74	1208.56	−24.2	0.95	3.8	Th	5
68R	1	40–42	1210.10	−32.4	1.59	4.8	AF	5
Site 1185A								
8R	1	87–89	309.27	−18.3	12.00	1.4	Th	1
8R	2	20–22	310.10	−41.9	5.12	1.3	Th	2
8R	2	58–60	310.48	−40.8	18.70	2.1	Th	2
8R	2	108–110	310.98	−36.9	13.24	1.0	AF	2

Table 1 (*Continued*).

Core	Section	Interval (cm)	Depth (mbsf)	Inclination (°)	Intensity (mA m^2/kg)	MAD (°)	Demag type	Inclination group
9R	1	12–14	317.12	−39.7	6.96	2.6	Th	2
9R	2	21–23	318.71	−49.9	4.76	0.9	Th	3
9R	2	54–56	319.04	−44.2	7.75	1.9	AF	3
9R	2	71–73	319.21	−42.2	3.20	1.2	Th	3
9R	2	104–106	319.54	−46.2	2.44	0.9	Th	3
9R	3	14–16	320.12	−42.5	2.15	2.0	Th	3
9R	3	66–71	320.64	−49.1	1.47	1.5	Th	3
9R	3	126–128	321.24	−50.3	1.74	1.1	Th	3
10R	1	81–83	323.41	−41.1	5.13	1.8	Th	3
10R	1	103–105	323.63	−44.8	3.99	1.0	AF	3
10R	2	17–19	324.15	−48.1	1.90	0.8	AF	3
10R	2	39–41	324.37	−44.3	2.42	1.6	AF	3
10R	3	32–34	325.59	−41.4	0.19	3.2	AF	3
10R	3	39–41	325.66	−45.4	2.15	2.7	Th	3
11R	1	50–52	328.20	−37.7	4.10	3.6	Th	3
11R	1	62–64	328.32	−42	3.55	6.7	Th	3
Site 1185B								
3R	2	6–8	317.16	−44	3.43	1.2	Th	1
3R	2	46–48	317.56	−42.3	2.21	1.1	Th	1
3R	2	73–75	317.83	−53.7	2.48	2.0	Th	1
3R	2	103–105	318.13	−45.1	3.92	1.6	Th	1
4R	1	31–33	319.51	−38.3	11.30	1.4	Th	2
4R	2	19–21	320.89	−37.2	2.79	1.4	Th	2
4R	3	45–47	321.62	−47.2	13.10	0.4	Th	3
4R	3	71–73	321.88	−45.5	5.28	1.4	Th	3
4R	3	100–102	322.17	−41.9	3.76	1.2	Th	3
4R	4	29–31	322.82	−45.3	4.43	1.6	Th	3
4R	4	110–112	323.63	−43.5	4.04	1.1	Th	3
4R	4	131–133	323.84	−46.9	4.53	3.3	Th	3
4R	6	24–26	325.45	Unstable			Th	
4R	6	76–78	325.97	−40.7	13.00	1.3	Th	3
4R	6	102–104	326.23	−44.4	2.67	1.1	Th	3
5R	1	26–28	329.06	−39.36	3.84	1.4	Th	4
5R	2	50–52	330.37	−38.4	8.96	1.3	Th	4
5R	3	94–96	332.22	−39.1	4.52	1.8	Th	4
5R	4	117–119	333.53	−49.2	1.15	2.7	Th	4
5R	5	97–99	334.60	−39.9	3.75	1.7	Th	4
5R	6	24–26	335.37	−41	2.84	3.2	Th	4
5R	7	26–28	33–6.84	−40.6	3.75	1.0	Th	4
5R	7	41–43	336.99	−40	4.06	1.1	AF	4
5R	7	105–107	337.63	−47.8	8.03	1.5	Th	5
5R	7	142–144	338.00	−50.7	4.58	0.7	Th	5
5R	8	3–5	338.07	−43.6	5.00	1.3	Th	5
6R	2	43–45	339.90	−34.1	2.24	0.6	AF	6
6R	3	92–94	341.45	−40.5	1.75	3.5	AF	6
6R	4	32–34	342.24	Unstable			Th	
6R	4	139–141	343.31	−40.2	1.17	2.5	Th	6
6R	5	3–5	343.38	−37.6	3.37	2.7	AF	6
6R	5	133–135	344.68	−38.2	1.06	3.1	Th	6
6R	6	68–70	345.48	−40.7	1.54	1.6	Th	6
7R	2	79–81	350.39	−33.3	8.00	0.9	Th	6
7R	2	102–104	350.62	−44	3.16	0.9	Th	6
7R	2	116–118	350.76	−37.9	6.29	1.9	Th	6

Table 1 (*Continued*).

Core	Section	Interval (cm)	Depth (mbsf)	Inclination (°)	Intensity (mA m^2/kg)	MAD (°)	Demag type	Inclination group
7R	3	16–18	351.26	−45.4	6.26	0.7	Th	7
7R	3	74–76	351.84	−42.7	3.03	1.6	AF	7
7R	4	10–12	352.59	−41.6	6.18	1.5	Th	7
8R	1	30–32	358.00	−46.1	5.59	0.7	Th	7
8R	1	96–98	358.66	−38.6	4.35	0.7	AF	7
9R	1	77–79	368.07	−44.2	7.39	0.9	Th	7
9R	3	36–38	370.52	−48.3	1.78	1.2	AF	7
10R	2	7–9	378.43	−43.1	6.85	1.3	Th	7
11R	1	108–110	387.58	−39.1	4.02	1.5	Th	8
12R	1	20–22	396.30	−34.8	3.54	1.1	Th	8
12R	1	47–49	396.57	−28.7	3.13	2.0	AF	9
12R	1	84–86	396.94	−22.4	6.59	1.2	Th	9
14R	1	85–87	406.55	−39.1	4.28	2.1	Th	10
14R	2	40–42	407.60	−46.9	7.34	1.5	Th	10
14R	2	135–137	408.55	−26.6	3.01	0.7	Th	11
14R	3	54–56	409.24	−33	2.47	1.9	Th	11
15R	1	65–67	415.95	−41.6	5.41	1.4	Th	12
15R	2	18–20	416.98	−46.1	4.32	0.6	AF	12
15R	2	137–139	418.17	−44	2.45	1.9	AF	12
15R	3	57–59	418.78	−39.2	5.53	1.1	Th	12
16R	1	40–42	425.30	−36	5.68	0.8	AF	12
16R	1	101–103	425.91	−41.5	3.59	0.9	Th	12
17R	1	66–68	435.26	Unstable			Th	
17R	2	55–57	436.25	Unstable			AF	
17R	3	77–79	437.88	Unstable			Th	
17R	4	42–44	438.96	−45.4	7.95	1.1	AF	13
18R	1	123–125	445.53	Unstable			Th	
19R	1	37–39	449.47	−50.1	4.13	1.8	AF	13
19R	2	78–80	451.33	−49.8	3.78	3.9	Th	13
19R	2	112–114	451.67	−49.3	2.82	1.2	Th	13
19R	3	100–102	453.00	−50.5	1.59	1.4	AF	13
19R	4	72–74	453.76	−53.3	2.04	2.6	Th	13
20R	2	23–25	455.38	−56.2	5.30	1.1	AF	13
20R	3	72–74	457.15	−49.1	9.45	2.3	Th	13
21R	3	41–43	466.26	−58.6	3.63	1.2	AF	13
21R	5	109–111	46–9.52	−50.7	10.90	3.1	Th	13
21R	7	36–38	471.58	−51.5	18.20	2.6	Th	13
21R	8	69–71	473.33	−54.5	6.11	1.1	AF	13
22R	1	107–109	474.27	Unstable			Th	
22R	2	83–85	475.39	Unstable			Th	
22R	3	132–134	477.28	Unstable			AF	
22R	4	70–72	478.03	−51.2	3.14	3.9	Th	13
22R	6	82–84	481.12	Unstable			AF	
23R	2	89–91	485.19	Unstable			Th	
24R	1	137–139	493.87	Unstable			Th	
28R	1	18–20	517.78	−53.5	2.78	9.0	AF	13
28R	1	44–46	518.04	−53.1	2.47	3.9	Th	13
28R	1	85–87	518.45	−49.7	3.11	2.7	AF	13
Site 1186								
30R	2	17–19	967.93	−46.3	1.56	2.9	AF	1
30R	2	33–35	968.09	−51.6	1.25	2.6	Th	1
30R	2	69–71	968.45	−48.0	2.94	2.4	AF	1
31R	1	32–34	970.32	−45.6	3.78	4.3	Th	1

Table 1 (*Continued*).

Core	Section	Interval (cm)	Depth (mbsf)	Inclination (°)	Intensity (mA m^2/kg)	MAD (°)	Demag type	Inclination group
31R	1	67–69	970.67	−53.5	2.31	2.0	AF	1
31R	2	90–92	972.39	Unstable			Th	
31R	3	6–8	972.82	−50.7	4.36	3.4	Th	1
31R	3	99–101	973.75	−41.6	2.19	3.7	AF	2
31R	4	45–47	974.31	Unstable			Th	
32R	1	24–26	976.44	Unstable			Th	
32R	1	65–67	976.85	−37.0	3.19	4.6	AF	2
32R	1	117–119	977.37	−30.8	0.77	4.7	Th	2
32R	2	3–5	977.70	−47.8	0.52	1.8	AF	3
32R	2	109–111	978.76	−45.6	1.25	4.2	AF	3
32R	3	31–33	979.48	−39.5	4.78	3.9	Th	4
32R	3	49–51	979.66	−36.1	1.84	6.2	AF	4
32R	3	134–136	980.51	Unstable			Th	
32R	4	60–62	981.26	Unstable			AF	
32R	4	79–81	981.45	Unstable			Th	
33R	1	9–11	981.09	Unstable			Th	
33R	1	47–49	981.47	−48.0	3.64	6.0	AF	5
33R	1	62–64	981.62	Unstable			Th	
33R	2	4–6	982.09	Unstable			Th	
33R	2	39–41	982.44	−39.5	4.33	4.7	AF	5
33R	2	53–55	982.58	Unstable			AF	
33R	2	59–61	982.64	Unstable			Th	
33R	2	115–117	98–3.20	−43.4	3.23	1.5	AF	5
33R	3	13–15	983.38	Unstable			Th	
33R	3	41–43	983.66	Unstable			AF	
34R	1	3–5	985.83	Unstable			Th	
34R	1	134–136	987.14	−43.2	7.99	4.2	AF	5
34R	2	25–27	987.48	Unstable			Th	
34R	2	72–74	987.95	Unstable			AF	
34R	2	100–102	988.23	Unstable			Th	
34R	3	4–6	988.73	Unstable			Th	
34R	3	54–56	989.23	Unstable			AF	
34R	3	89–91	989.58	Unstable			Th	
34R	4	69–71	990.88	Unstable			Th	
34R	4	106–108	991.25	Unstable			AF	
34R	5	96–98	992.65	Unstable			Th	
34R	6	2–4	993.19	−40.7	9.22	1.6	AF	6
34R	6	28–30	993.45	−37.3	7.12	1.6	Th	6
35R	1	56–58	996.06	−39.0	7.70	2.4	AF	6
35R	1	62–64	996.12	−38.9	9.19	5.9	Th	6
35R	1	95–97	996.45	−33.1	5.59	2.9	AF	6
37R	1	48–50	1015.28	−44.5	10.80	5.5	Th	7
37R	1	79–81	1015.59	−53.1	14.30	1.0	AF	7
37R	1	112–114	1015.92	−52.0	5.54	5.2	AF	7
37R	2	29–31		Unstable			AF	
37R	2	35–37	1016.60	−47.0	8.20	3.4	Th	7
37R	2	51–53	1016.76	−49.0	6.29	1.9	AF	7
37R	3	3–5	1016.86	−38.9	8.66	5.3	Th	7
37R	3	29–31	1017.12	Unstable			AF	
37R	3	115–117	1017.98	Unstable			Th	
38R	1	10–12	1019.50	Unstable			AF	
38R	1	117–119	1020.57	Unstable			Th	
38R	1	140–142	1020.80	Unstable			AF	

Table 1 (*Continued*).

Core	Section	Interval (cm)	Depth (mbsf)	Inclination (°)	Intensity (mA m^2/kg)	MAD (°)	Demag type	Inclination group
38R	2	49–51	1021.34	Unstable			Th	
38R	2	124–126	1022.09	−52.2	5.52	2.7	AF	7
38R	3	3–5	1022.33	Unstable			Th	
38R	3	66–68	1022.96	−60.8	8.19	2.5	AF	7
38R	3	106–108	1023.36	−51.1	5.63	3.7	AF	7
38R	4	18–20	1023.90	−52.6	7.16	6.0	Th	7
38R	4	109–111	1024.81	Unstable			AF	
38R	4	131–133	1025.03	Unstable			Th	
39R	1	7–9	1024.47	Unstable			AF	
39R	1	62–64	1025.02	Unstable			Th	
39R	1	101–103	1025.41	−48.6	1.56	7.9	AF	7
39R	2	2–4	1025.74	Unstable			AF	
39R	2	73–75	1026.45	Unstable			Th	
39R	3	53–55	1027.42	−51.0	0.88	4.3	Th	7
39R	3	94–96	1027.83	−60.4	3.66	1.3	AF	7
39R	3	131–133	1028.20	−50.9	3.37	2.7	Th	7
39R	4	16–18	1028.51	Unstable			Th	
39R	4	51–53	1028.86	−54.0	3.89	1.4	AF	7
39R	4	90–92	1029.25	−45.8	5.11	2.7	AF	7
39R	5	34–36	1029.75	−59.9	7.95	1.6	Th	7
39R	5	53–55	1029.94	Unstable			AF	
Site 1187A								
2R	2	86–88	367.54	−45.0	1.29	0.7	AF	1
2R	2	116–18	367.84	−37.7	1.28	1.1	AF	1
3R	1	81–83	375.31	−45.9	0.97	1.0	AF	1
3R	2	54–56	376.50	−41.7	3.04	0.7	AF	1
3R	3	32–34	377.76	−38.0	1.98	0.9	AF	1
3R	3	64–66	378.08	−41.8	1.25	0.8	AF	1
3R	4	9–11	378.98	−45.8	1.14	0.4	AF	1
4R	1	25–27	384.45	−33.6	1.52	0.5	AF	1
4R	2	94–96	386.63	−50.9	2.02	0.7	AF	2
4R	3	136–138	388.55	−43.9	2.71	1.0	AF	2
4R	4	60–62	389.29	−47.3	1.60	0.7	AF	2
4R	5	137–139	391.23	−48.9	0.76	1.1	AF	2
4R	6	28–30	391.64	−51.7	2.23	0.7	AF	2
5R	1	21–23	394.01	−39.3	1.37	1.2	AF	3
5R	1	66–68	394.46	−33.0	1.07	1.2	AF	3
5R	2	80–82	395.98	−42.5	1.41	0.9	AF	3
5R	3	90–92	397.58	−32.3	1.65	1.2	AF	3
5R	4	78–80	398.89	−44.1	1.48	0.5	AF	4
5R	4	120–122	399.31	−47.9	2.11	1.1	AF	4
5R	6	98–100	402.09	−45.6	1.95	0.8	AF	4
5R	7	31–33	402.71	−39.3	2.36	1.0	AF	4
6R	1	49–51	403.89	−41.8	0.99	0.5	AF	4
6R	2	108–110	405.71	−39.1	1.83	0.9	AF	4
6R	3	110–112	407.23	−43.8	1.29	1.0	AF	4
6R	4	45–47	408.03	−39.7	1.49	0.7	AF	4
6R	5	2–4	408.19	−42.1	0.49	1.5	AF	4
6R	5	19–21	408.36	−40.4	1.90	0.8	AF	4
6R	5	33–35	408.50	−41.0	1.28	1.1	AF	4
6R	5	44–46	408.61	−40.2	1.19	0.8	AF	4
6R	5	58–60	408.75	−40.4	1.77	1.1	AF	4
6R	5	68–70	408.85	−41.0	0.75	1.0	AF	4

Table 1 (*Continued*).

Core	Section	Interval (cm)	Depth (mbsf)	Inclination (°)	Intensity (mA m^2/kg)	MAD (°)	Demag type	Inclination group
6R	5	79–81	408.96	−41.6	1.31	1.0	AF	4
6R	5	89–91	409.06	−42.6	2.98	1.2	AF	4
6R	5	106–08	409.23	−41.9	1.12	0.5	AF	4
6R	5	116–118	409.33	−43.0	0.72	1.4	AF	4
6R	6	56–58	410.09	−42.0	1.33	0.6	AF	4
6R	7	65–67	411.49	−46.9	3.27	1.0	AF	5
7R	1	14–16	413.14	−48.9	1.09	1.0	AF	5
7R	2	80–82	415.27	−47.6	1.21	1.0	AF	5
7R	3	109–111	416.82	−27.7	0.82	1.5	AF	6
7R	4	14–16	417.06	−35.5	0.75	0.4	AF	6
7R	4	32–34	417.24	−34.6	0.86	1.1	AF	6
7R	6	30–32	419.60	−35.1	1.59	0.9	AF	7
7R	7	98–100	421.31	−39.1	3.48	0.6	AF	7
8R	1	34–36	422.94	−40.6	1.98	0.9	AF	7
8R	2	64–66	424.63	−44.8	0.89	1.3	AF	8
8R	3	58–60	425.92	−34.1	2.87	0.6	AF	8
8R	4	105–107	427.88	−41.0	2.18	1.1	AF	8
8R	5	116–118	429.30	−44.6	0.93	0.7	AF	8
8R	6	72–74	430.22	−45.8	1.55	1.0	AF	8
8R	7	14–16	431.01	−39.5	1.51	0.9	AF	8
9R	1	32–34	432.62	−39.5	1.14	1.0	AF	8
9R	2	14–16	433.82	−50.4	1.11	0.4	AF	8
9R	3	91–93	436.00	−40.9	2.49	0.7	AF	8
9R	4	101–102	437.11	−42.8	2.16	0.8	AF	8
9R	5	6–8	437.57	−35.2	2.73	1.0	AF	8
9R	5	82–84	438.33	−43.5	3.02	0.9	AF	8
9R	6	49–51	439.46	−43.7	1.09	0.9	AF	8
9R	7	15–17	440.58	−49.2	2.17	0.7	AF	8
10R	1	12–14	442.02	−45.7	1.50	1.0	AF	8
10R	2	67–69	444.07	−46.9	1.86	0.5	AF	8
10R	3	62–64	445.52	−33.2	3.36	0.5	AF	9
10R	4	119–121	447.31	−36.0	3.51	0.7	AF	9
10R	5	17–19	447.58	−32.8	3.43	1.6	AF	9
10R	5	40–42	447.81	−35.0	2.41	0.6	AF	9
10R	6	41–43	448.73	−36.4	1.70	0.8	AF	9
10R	7	9–11	449.68	−39.5	3.31	0.5	AF	9
11R	1	103–105	452.53	−40.1	1.75	0.6	AF	9
11R	2	30–32	453.00	−35.6	1.91	0.5	AF	9
11R	3	2–4	454.22	−41.4	1.05	0.8	AF	9
11R	3	78–80	454.98	−39.9	1.27	1.3	AF	9
11R	4	32–34	455.52	−41.4	3.21	0.3	AF	9
11R	5	31–33	456.91	−37.1	2.87	0.5	AF	9
11R	5	125–127	457.85	−42.4	0.92	0.9	AF	9
11R	6	35–37	458.39	−30.9	2.04	1.5	AF	9
12R	1	18–20	461.28	−42.7	1.09	0.7	AF	9
12R	2	44–46	463.02	−42.1	2.13	2.5	AF	9
12R	3	45–47	464.49	−33.5	1.42	1.7	AF	10
12R	3	99–101	465.03	−39.7	0.69	2.4	AF	10
12R	4	105–107	466.44	−33.0	1.11	0.8	AF	10
12R	5	44–46	466.99	Unstable			Th	
12R	5	79–81	467.34	−34.1	1.44	0.9	AF	10
13R	1	105–107	471.75	−40.4	1.93	0.5	AF	10
13R	2	31–33	472.30	−31.3	2.24	1.7	AF	10

Table 1 (*Continued*).

Core	Section	Interval (cm)	Depth (mbsf)	Inclination (°)	Intensity (mA m^2/kg)	MAD (°)	Demag type	Inclination group
13R	3	103–105	474.41	Unstable			Th	
13R	4	6–8	474.73	−36.0	1.49	0.8	AF	10
13R	4	95–97	475.62	−31.8	1.26	1.2	AF	10
13R	5	63–65	476.30	−38.4	2.39	1.2	AF	10
13R	6	115–117	478.32	−44.3	1.15	0.6	AF	11
14R	2	36–38	482.16	−50.6	1.13	0.6	AF	11
14R	3	28–30	483.46	−34.6	1.88	0.5	AF	12
14R	4	7–9	484.75	−37.7	1.98	1.0	Th	12
15R	2	37–39	491.22	−34.0	3.09	0.3	Th	12
15R	3	41–43	492.53	−16.7	1.18	1.5	Th	13
15R	3	88–90	493.00	−26.3	1.63	0.6	AF	13
15R	4	20–22	493.67	−32.3	8.83	0.5	AF	13
15R	4	54–56	494.01	−19.4	3.02	0.4	Th	13
16R	1	46–48	500.16	−37.3	1.65	0.4	Th	14
16R	2	63–65	501.27	−39.6	1.49	0.5	Th	14
16R	4	12–14	503.48	−42.6	1.48	1.1	Th	14
16R	5	90–92	505.72	−37.6	1.72	0.5	Th	14

(55.2% average recovery) we obtained 331 azimuthally unoriented paleomagnetic samples.

3. Results

3.1. Experimental procedures

Temperature dependence of initial susceptibility $k(T)$ was measured in argon atmosphere using a KLY-2 susceptibility meter equipped with a furnace. All measured samples are characterized by the presence of titanomaghemite, evidenced by irreversible destruction of a magnetic phase at ~300°C during $k(T)$ experiments. Although titanomaghemite carries a chemical remanent magnetization (CRM) produced during post-emplacement hydrothermal alteration, the direction of the CRM is inherited from the primary thermal remanent magnetization of the primary titanomagnetite [22]. The presence of titanomaghemite is therefore not significant for the paleodirectional studies.

Detailed alternating field (AF) and thermal step-wise demagnetizations were performed at the paleomagnetic laboratories at the University of California at Santa Cruz, University of Houston, and University of Munich. Data from different laboratories are found to be in excellent agreement with each other. Based on the demagnetization data the characteristic remanent magnetization (ChRM) directions were calculated using principal component analysis [23]. Only ChRM components based on four or more demagnetization steps, pointing towards the origin, and having a maximum angular deviation (MAD) less than 10° were accepted for further analyses. Typical examples of accepted and rejected samples are shown in Fig. 2. Out of the altogether 331 paleomagnetic specimens, 270 satisfy the above-mentioned acceptance criteria; further details are listed in Table 1. We note that a large majority of accepted samples yield well-defined ChRM inclinations with MAD values much less than 10° (Fig. 2c and Table 1). Rejected demagnetization results stem from samples that altered significantly during thermal cleaning and/or samples in which a strong drill-induced overprint cannot be removed in step-wise demagnetization (Fig. 2d). In cases when thermal and AF demagnetization data can be directly compared, the data are in excellent agreement (Fig. 2). A small reversed component often observed in the 250–350°C interval during thermal demagnetization (Fig. 2a) is not observed in AF demagnetization (Fig. 2b) and we speculate that this phenomenon relates to titanomaghemite. We always define the ChRM direction based on the higher temperature steps.

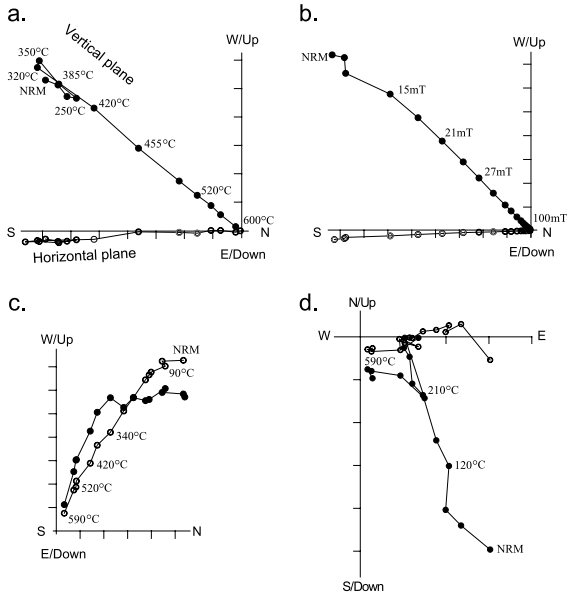

Fig. 2. Orthogonal vector plots of selected samples. (a) Thermal and (b) AF demagnetizations on the same paleomagnetic sample (1185A-9R-03W, 126–128 cm) cut into two halves are in excellent agreement. (c) Slightly noisy but acceptable sample (1186-31R-03W, 6–8 cm) with MAD = 3.4°. (d) Rejected sample (1186-38R-01W, 117–119 cm) with a strong vertical (drill-induced) overprint.

3.2. Inclination groups

Due to the limited recovery it is not straightforward to define individual lava flows and cooling units based on visual inspection of the cores. The definition of inclination groups (i.e. independent spot readings of the field) therefore has to some extent to rely on the paleomagnetic data themselves (see also [5,24,25]) (Figs. 3–6). The significance of the ODP Leg 192 igneous units [8] is particularly problematic for the pillow basalts, where the number of cooling units (pillows) is much larger than the number of igneous units. For example, the 12 igneous units of Site 1187 (Fig. 6) contain as many as 146 basaltic pillows with an average thickness of only 61 cm [8]. For these reasons some of the inclination groups are defined based only on the paleomagnetic data, and as a consequence several of the igneous units contain more than one inclination group (Figs. 3–6). The inclination groups agree excellently with igneous unit boundaries, when these boundaries are clearly defined by, for example, inter-basaltic sediments. The mean inclination for each group is calculated based on the statistical procedures of [26] using the pmag software package [27]. The inclination groups are supported by Z-statistics [28], showing that all consecutive inclination groups are statistically distinct.

All samples and inclination groups have negative inclinations, i.e. normal polarity. Although it has been suggested that the OJP formed shortly after the onset of the Cretaceous normal superchron [7,29], the uncertainties in the age of the OJP as well as the Early Cretaceous geomagnetic polarity time scale (GPTS; [30]) do not allow a unique correlation to the GPTS. The inclination groups are listed in Table 2 for each of the four sites.

3.3. Paleosecular variation

Before the paleomagnetic paleolatitudes can be used for paleogeographic reconstructions (Section 3.4) it is important to ensure that paleosecular variation has been averaged out so that the site-mean inclination represents a time-averaged geocentric axial dipole field. Following standard procedures we estimate paleosecular variation as the angular standard deviation (ASD) of the inclination groups transformed into pole space [31]. The ASD values range between 9° and 14° (Table 3), which is in good accordance with the paleosecular variation (8°–13°) predicted by the model of [32] for the Early Cretaceous, suggesting that paleosecular variation has been averaged out. However, as pointed out by [5], it is important to note that ASD values depend on the non-unique definition of inclination groups (Section 3.2) and it is therefore difficult to ascertain that paleosecular variation has been fully averaged out based solely on ASD analysis.

3.4. Paleolatitude

The four site-mean inclinations and their corresponding paleolatitudes (Table 3) represent a unique Pacific paleomagnetic dataset, which allows us to discuss uncertainties not easily detected

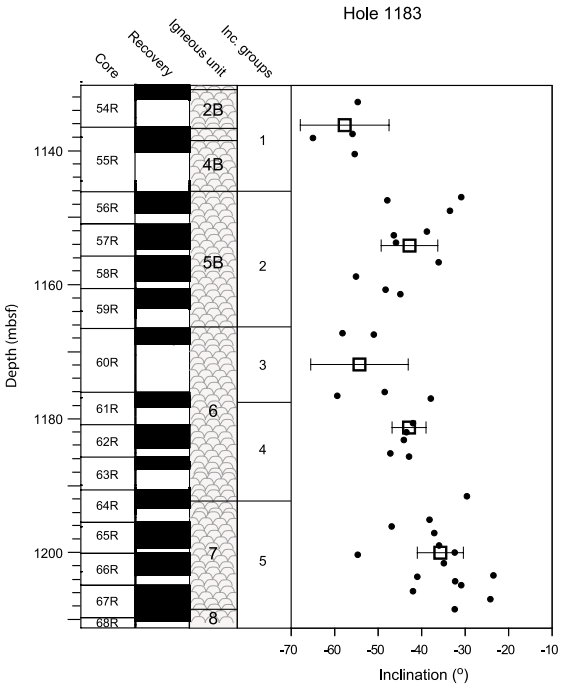

Fig. 3. Site 1183 downhole variation in ChRM inclination. A total of 80.7 m of basalt flows and pillows was drilled; 39 samples out of 46 were used. Small circles show inclination values for individual samples and larger open squares show the mean inclination for each inclination group, with error bars denoting α_{95} (95% confidence).

at individual drill sites. The fact that all four site-mean inclinations are statistically indistinguishable strongly suggests that paleosecular variation has been averaged out at the individual sites (Section 3.3). Although the OJP drill sites are distributed across the plateau from its crest to its flanks (Fig. 1), the statistically indistinguishable site-mean inclinations further indicate that the studied basalts have suffered little or no tectonic disturbance since their emplacement. Because the Leg 192 sites are geographically closely spaced (Fig. 1), the inclination data can be combined to obtain a mean Leg 192 inclination of −41.4° with an α_{95} of 2.6° (Table 3). We note that although our definition of inclination groups is not unique, only the ASD and α_{95} values vary for different divisions. The mean Leg 192 inclination, on the other hand, is very robust with respect to different divisions. If all samples are treated as independent readings we obtain a statistically indistinguishable mean inclination of −42.4°.

In order to compare our paleomagnetic inclination data with other Pacific data it is necessary to transform the results into pole space. Since the data are azimuthally unoriented, a paleomagnetic pole cannot be defined, it must, however, lie on a small circle centered on the site and with a radius of the paleomagnetic paleo-colatitude. As shown in Fig. 7, the paleo-colatitudes of the four Leg 192 sites are in good accordance with that of Site 807 (ODP Leg 130; [21]) drilled in the more northern part of the OJP. This further supports that paleosecular variation has been averaged and that

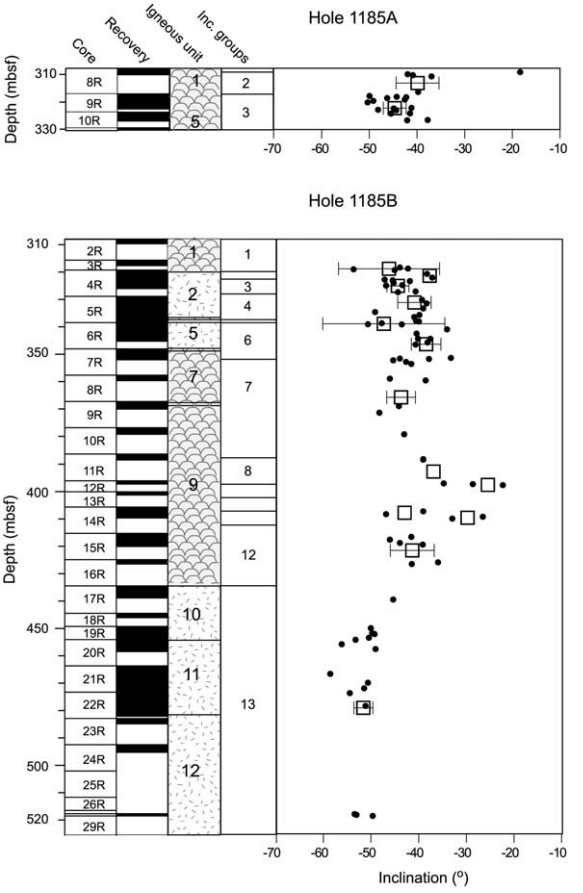

Fig. 4. Site 1185 downhole variation in ChRM inclination for (a) hole 1185A and (b) hole 1185B. At hole 1185A, 16.7 m and at hole 1185B, 216.6 m of basalt flows and pillows was drilled; 93 samples out of 105 were used. Same notation as in Fig. 3.

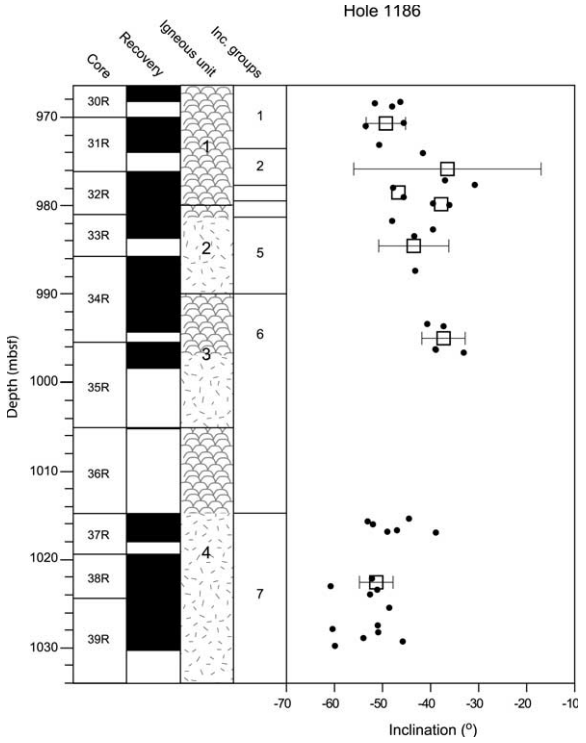

Fig. 5. Downhole variation in ChRM inclination for hole 1186A. A total of 65.4 m of basalt flows and pillows was drilled; 39 samples out of 79 were used. Same notation as in Fig. 3.

there is no unrecognized tectonic tilting of the basalt sequence at the four Leg 192 sites or Site 807. The only other Pacific Early Cretaceous basaltic paleomagnetic paleolatitude estimates are from the ~130 Ma Mid-Pacific Mountains (ODP Site 866; [33]), and the ~124 Ma MIT Guyot (ODP Site 878; [34]) (Fig. 7). These paleo-colatitudes are discordant from the OJP ones, which could reflect unrecognized tectonic tilting of the basalt sequence at these sites, emphasizing the importance to test data with multiple sites. Moreover, these two sites formed closer to the paleo-equator, which makes it more difficult to unambiguously discern between normal, intermediate, and reverse polarities present in these two sites. Finally, the $^{40}Ar/^{39}Ar$ ages reported for these two sites may be too young as whole-rock $^{40}Ar/^{39}Ar$ geochronology is difficult on altered ocean floor basalts, often yielding ages that are too young [10].

4. Discussion

4.1. The Pacific APWP

The use of relative plate motion circuits to transfer paleomagnetic data from one lithospheric plate to another has led to significant improvements of the APWPs for almost all major lithospheric plates [4]. The Pacific plate is the major exception, as the dominantly convergent circum-Pacific plate boundaries exclude plate circuit models, except a problematic one including the South Pacific and Antarctica [1]. Moreover, it is difficult to obtain Pacific geological material suitable for direct paleomagnetic studies, and the most recent updates of the Pacific APWP, therefore, rely almost exclusively on indirect paleomagnetic poles derived from seamount magnetic anomaly modeling [35] and skewness of marine magnetic anomalies [36]. The fact that several of the indirect APWP poles are mutually inconsistent (Fig. 8)

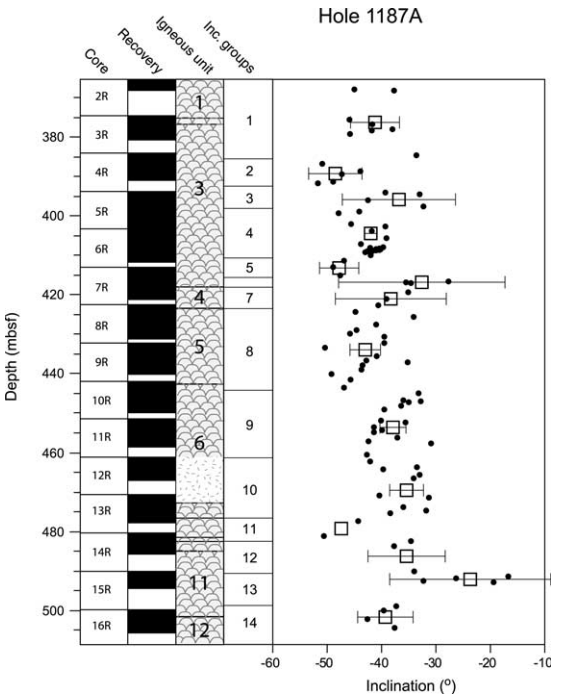

Fig. 6. Downhole variation in ChRM inclination for hole 1187A. A total of 135.8 m of basalt flows and pillows was drilled; 99 samples out of 101 were used. Same notation as in Fig. 3.

Table 2
Inclination group averages

Inclination group	Number of samples	Inclination (°)	α_{95} (°)	K
1183				
1	4	−57.7	10.2	139
2	10	−42.8	6.5	56
3	4	−54.3	11.2	115
4	6	−42.9	3.9	356
5	15	−35.7	5.3	49
1185A				
1	1	−18.3		
2	4	−39.8	4.5	712
3	15	−44.6	2.4	250
1185B				
1	4	−46.3	10.6	127
2	2	−37.7		
3	8	−44.4	2.3	624
4	8	−40.9	3.5	278
5	3	−47.4	12.8	257
6	9	−38.5	3.1	293
7	8	−43.8	3	372
8	2	−36.9		
9	2	−25.5		
10	2	−43		
11	2	−29.8		
12	6	−41.4	4.6	261
13	17	−51.7	2	
1186				
1	6	−49.3	4.1	333
2	3	−36.5	19.5	112
3	2	−46.7		
4	2	−37.8		
5	4	−43.5	7.3	271
6	5	−37.3	4.5	393
7	17	−51.3	3.5	100
1187				
1	8	−41.2	4.5	166
2	5	−48.5	4.9	339
3	4	−36.8	10.4	134
4	19	−42	1.2	669
5	3	−47.8	3.6	3187
6	3	−32.6	15.3	180
7	3	−38.3	10.2	406
8	16	−43	2.8	162
9	16	−37.9	2.4	230
10	9	−35.4	3.1	280
11	2	−47.4		
12	3	−35.4	7.1	833
13	4	−23.7	14.8	67
14	4	−39.3	5.1	551

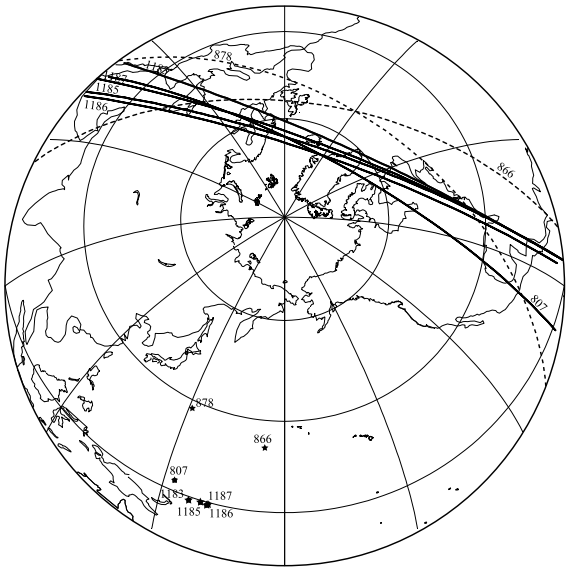

Fig. 7. The studied ODP drill sites (stars) and their corresponding paleo-colatitudes (small circles). Also shown are the previous ODP Site 807 drilled into the northern portion of the OJP [7] as well as Sites 866 [33] and 878 [34]. The excellent agreement for the five different OJP drill sites is evident from the paleo-colatitudes lying close to each other (and crossing each other). The close proximity of the paleo-colatitudes demonstrates that the studied basalts have suffered little or no tectonic disturbance since their emplacement.

has been interpreted to indicate either very fast TPW [35] or that some of the indirect APWP poles contain undetected errors related to induced or secondary magnetizations [37].

Paleomagnetic data derived from detailed demagnetization experiments on basaltic drill cores allow definition of the primary magnetization and these data are therefore advantageous compared to indirect Pacific paleomagnetic data. The reliability of paleomagnetic data from single basaltic drill sites is, however, not straightforward, as non-averaged paleosecular variation and local tectonics could yield erroneous results [5]. The fact that the paleomagnetic results presented in this study are supported by data from four individual sites (Fig. 7) strongly suggests that the mean OJP paleo-colatitude (Fig. 8) represents a time-averaged field and that the studied basalts have suffered little or no tectonic disturbance since their emplacement. The OJP paleo-colatitude is statistical-

Table 3
Site-mean inclinations and paleolatitudes

Site	*N*/*n*	Inc. (°)	*k*	α_{95} (°)	Paleolat. (°N)	ASD (°)
807	14/75	−33.2	34.8	6.6	$-18.1\ ^{-4.5}/_{+4.0}$	12.7
1183	5/39	−46.7	40.0	14.3	$-27.9\ ^{-14.2}/_{+10.4}$	13.9
1185	15/93	−40.8	74.0	4.3	$-23.3\ ^{-3.3}/_{+2.0}$	9.4
1186	7/39	−43.2	88.0	6.9	$-25.2\ ^{-5.7}/_{+5.0}$	8.9
1187	14/99	−39.2	74.0	4.5	$-22.2\ ^{-3.4}/_{+3.1}$	9.3
All Leg 192	41/270	−41.4	66.0	2.6	$-23.8\ ^{-2.0}/_{+1.9}$	10.1

N/*n* is number of inclination groups/samples; Inc. is the mean inclination of the site; *k* and α_{95} are statistical parameters; Paleolat. is the paleomagnetic paleolatitude; ASD is angular standard deviation. Given in the top row are the previous Site 807 results [21].

ly distinct from the combined 125 Ma APWP pole (Fig. 8) based on skewness data (45%), seamount magnetic anomaly modeling (27%), and direct paleomagnetic data from some few very short basalt cores (28%). It is not easy to reconcile this difference as a result of the 5 Ma difference in age, possible non-dipole fields and/or TPW. We note that previously published direct paleomagnetic data from ~80 Ma Pacific basalts have found similar differences between the corresponding paleo-colatitude and contemporaneous indirect Pacific APWP poles [24]. The OJP paleo-colatitude data therefore extend the suggestion that the reliability of some Pacific APWP poles may be questionable [24].

The Pacific APWP has been used to suggest that plate circuit models linking South Africa with the Pacific are problematic [1]. New magnetic lineation data from the South Pacific [38] have significantly improved this plate circuit and based on these new data it is possible to transfer the 0–90 Myr part of the South African APWP to the Pacific plate (Fig. 8). Unfortunately, it is not possible to transfer South African APWP poles older than 90 Ma and it is therefore not possible to directly compare the rotated South African APWP with the OJP paleo-colatitude. We do, however, note that the rotated APWP is in excellent agreement with the ~80 Ma paleo-colatitude obtained from basalts drilled at Detroit Seamount [24]. On the other hand, there is poor agreement between the rotated APWP and the Pacific APWP (Fig. 8). Although one could interpret this difference as evidence that the South African–Antarctica–Pacific plate reconstruction is wrong, we suggest that this difference simply reflects problems related to the Pacific APWP.

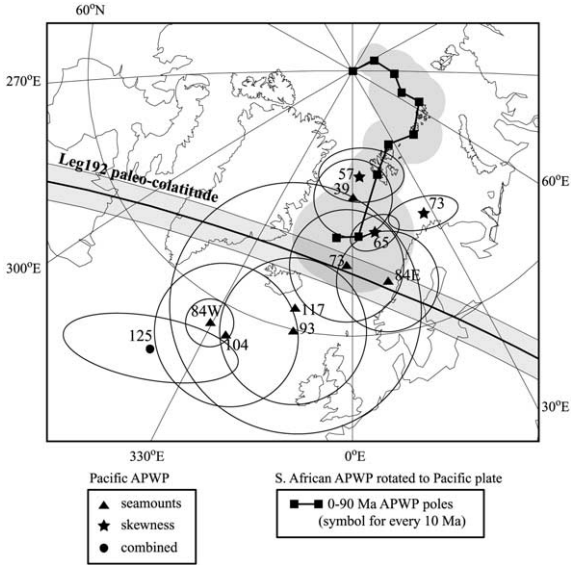

Fig. 8. Mean Leg 192 paleo-colatitude and corresponding 95% confidence interval (gray area). The paleomagnetic poles of the Pacific plate are based on seamount anomaly modeling (triangles; [35]), magnetic lineation skewness (stars; [36,49,50]), and a combination of different data sources (circle; [51]). Also shown are the 0, 10, 20, 30, 40, 50, 60, 70, 80, and 90 Ma South African APWP poles (squares; [4]) rotated to the Pacific plate using the rotation parameters listed in [42]. Note that the Pacific paleomagnetic poles are mutually inconsistent and significantly different from the rotated South African APWP. The 120 Ma mean paleo-colatitude obtained in this study is statistically distinct at the 95% confidence level from the combined 125 Ma APWP pole [51].

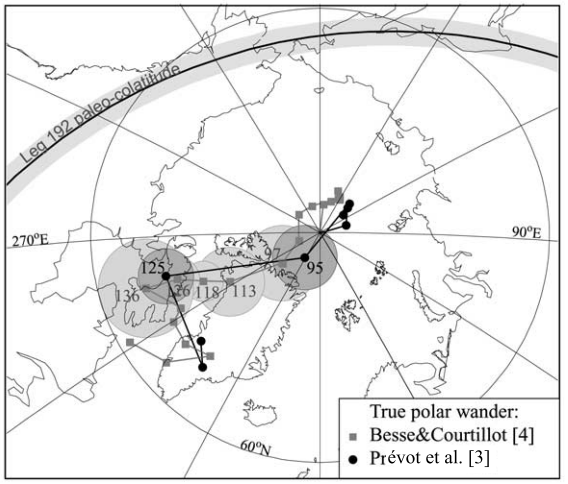

Fig. 9. The Leg 192 paleo-colatitude rotated according to the Pacific hotspot reconstruction [43]. The Pacific TPW pole must lie somewhere on the reconstructed paleo-colatitude. Note that the 95% confidence interval (gray area) around the reconstructed paleo-colatitude does not include uncertainties related to the hotspot reconstruction. Also shown are Indo-Atlantic TPW estimates [3,4]. The difference between Pacific and Indo-Atlantic TPW estimates is best explained by relative motion between Pacific and Indo-Atlantic hotspots (see text).

4.2. TPW or motion between hotspots?

Assuming that hotspots form a fixed reference frame, it is possible to estimate TPW, i.e. rotation of the entire solid Earth, as the differences between paleomagnetic and hotspot reconstructions [3,4]. Analysis of the Pacific hotspot tracks suggests that Pacific hotspots have remained fixed with respect to each other with relative motion of less than 2–3 mm/yr [39], i.e. less than 3° during 120 Myr. On the other hand, there is evidence of motion between Pacific and Indo-Atlantic hotspots [40–42], although these inferences are complicated by poor paleomagnetic control and difficulties in relative plate reconstructions. The new reliable Pacific paleomagnetic data presented here give us a possibility to test TPW estimates obtained from other lithospheric plates. First of all, we note that the paleomagnetic paleolatitude 23.8°S is ~20° north of the latitude suggested by reconstructions in an assumed fixed hotspot reference frame [43–46]. A consistent octupole term $g_3/g_1 = 0.1$ [47] will give a paleomagnetic paleolatitude ~4° lower than for a pure dipole field and a possible octupole field therefore cannot explain the difference. Hence either TPW and/or hotspot motion must be called upon.

As the OJP cannot be directly linked to the Louisville hotspot, Pacific TPW cannot be deduced by comparing the OJP paleomagnetic paleolatitude with the present latitude of the Louisville hotspot [2,7,21]. In Fig. 9 we have reconstructed the OJP paleo-colatitude with respect to Pacific hotspot tracks using the rotation poles of [43]. Although the exact location of the 120 Ma Pacific TPW pole cannot be defined, it must lie somewhere on the reconstructed paleo-colatitude. Comparing with the TPW estimates obtained from Indo-Atlantic hotspot and paleomagnetic data [3,4] it is clear that the Pacific TPW is inconsistent with the Indo-Atlantic one. The ~20° difference between the 120 Ma Indo-Atlantic TPW pole and the Pacific TPW paleo-colatitude (Fig. 9) supports the suggestion of significant motion between Pacific and Indo-Atlantic hotspots [40–42]. These new data cast serious doubt on the fixity of hotspots, and thereby the possibility to measure TPW by comparing paleomagnetic and hotspot data.

5. Conclusions

The mean paleomagnetic inclination of the four different ODP Leg 192 sites and a single Leg 130 site agree excellently, suggesting that paleosecular variation has been averaged out at each site and that the studied basalts are tectonically undisturbed. This unique dataset indicates that the Early Cretaceous part of the Pacific APWP may be wrong. The data also show that Pacific TPW is different from Indo-Atlantic TPW estimates, which strongly supports the suggestion of relative motion between Pacific and Indo-Atlantic hotspots [40–42]. Care must therefore be taken before differences between hotspot and paleomagnetic data are interpreted to reflect rotation of the entire solid Earth.

Acknowledgements

This research used samples provided by the Ocean Drilling Program (ODP). ODP is sponsored by the U.S. National Science Foundation (NSF) and participating countries under management of Joint Oceanographic Institutions (JOI), Inc. Funding for this research was provided by the Danish National Research Foundation (P.R.), U.S. Science Support Program of JOI (S.H.), and ODP/Germany Project Number So 72/70–1 (M.A.). Diana Dragoi performed parts of the laboratory experiments. Authors would like to thank Lynne Chambers and the scientific party of ODP Leg 192 for their invaluable comments. We are grateful to Trond Torsvik and Anthony Koppers for their constructive reviews. In our analysis we used software of Lisa Tauxe, Trond Torsvik and Mark Smethurst. *[RV]*

References

[1] G.A. Acton, R.G. Gordon, Paleomagnetic tests of Pacific plate reconstructions and implications for motion between hotspots, Science 263 (1994) 1246–1254.

[2] T.H. Torsvik, R. VanderVoo, T.F. Redfield, Relative hotspot motions versus True Polar Wander, Earth Planet. Sci. Lett. 202 (2002) 185–200.

[3] M. Prévot, E. Mattern, P. Camps, M. Daignieres, Evidence for a 20° tilting of the Earth's rotation axis 110 million years ago, Earth Planet. Sci. Lett. 179 (2000) 517–528.

[4] J. Besse, V. Courtillot, Apparent and true polar wander and the geometry of the geomagnetic field in the last 200 Myr, J. Geophys. Res. 107 (2002) 2300.

[5] W.W. Sager, Basalt core paleomagnetic data from Ocean Drilling Program Site 883 on Detroit Seamount, northern Emperor Seamount chain, and implications for the paleolatitude of the Hawaiian hotspot, Earth Planet. Sci. Lett. 199 (2002) 347–358.

[6] O. Eldholm, M. Coffin, Large igneous provinces and plate tectonics, in: M.A. Richards et al. (Eds.), The History and Dynamics of Global Plate Motions, AGU Monograph 121, 2000, pp. 309–326.

[7] J.A. Tarduno, W.V. Sliter, L. Kroenke, M. Leckie, H. Mayer, J.J. Mahoney, R. Musgrave, M. Storey, E.L. Winterer, Rapid formation of Ontong Java Plateau by Aptian mantle plume volcanism, Science 254 (1991) 399–403.

[8] J.J. Mahoney, J.G. Fitton, P.J. Wallace et al. (Eds), Proc. ODP Init. Reports 192 (2002).

[9] I.J. Parkinson, B.F. Schaefer, ODP Leg 192 Shipboard Scientific Party, A lower mantle origin for the world's biggest LIP? A high precision Os isotope isochron from Ontong Java Plateau basalts drilled on ODP Leg 192, EOS Trans. AGU 82, Fall Meet. Suppl. (2001) Abstract V51C-1030.

[10] L.M. Chambers, M.S. Pringle, J.G. Fitton, Age and duration of magmatism on the Ontong Java Plateau: $^{40}Ar/^{39}Ar$ results from ODP Leg 192, EOS Trans. AGU 83, Fall Meet. Suppl. (2002) Abstract V71B-1271.

[11] M.F. Coffin, L.M. Gahagan, Ontong-Java and Kerguelen plateaus - Cretaceous Icelands?, J. Geol. Soc. London 152 (1995) 1047–1052.

[12] C.R. Neal, J.J. Mahoney, L.W. Kroenke, R.A. Duncan, M. G. Petterson, The Ontong Java Plateau, in: J.J. Mahoney, M.F. Coffin (Eds.), Large Igneous Provinces, AGU Monograph 100, 1997, pp. 183–216.

[13] M.F. Coffin, O. Eldholm, Large igneous provinces: crustal structure, dimensions, and external consequences, Rev. Geophys. 32 (1994) 1–36.

[14] M.L.G. Tejada, J.J. Mahoney, C.R. Neal, R.A. Duncan, M.G. Petterson, Basement geochemistry and geochronology of central Malaita, Solomon islands, with implications for the origin and evolution of the Ontong Java Plateau, J. Petrol. 43 (2002) 449–484.

[15] M.A. Richards, R.A. Duncan, V.E. Courtillot, Flood basalts and hot-spot tracks - Plume heads and tails, Science 246 (1989) 103–107.

[16] A.D. Saunders, M. Storey, R.W. Kent, M.J. Norry, Consequences of plume-lithosphere interactions, in: B.C. Storey, T. Alabaster, R.J. Pankhurst (Eds.), Magmatism and the Causes of Continental Break-up, Spec. Publ. Geol. Soc. London 68 (1992) 41–60.

[17] E.J. Phinney, P. Mann, M.F. Coffin, T.H. Shipley, Sequence stratigraphy, structure, and tectonic history of the southwestern Ontong Java Plateau adjacent to the North Solomon Trench and Solomon Islands arc, J. Geophys. Res. 104 (1999) 20449–20466.

[18] J.J. Mahoney, M. Storey, R.A. Duncan, K.J. Spencer, M.S. Pringle, Geochemistry and age of the Ontong Java Plateau, in: M.S. Pringle, W.W. Sager, W.V. Sliter, S. Stein (Eds.), The Mesozoic Pacific: Geology, Tectonics, and Volcanism, AGU Monograph 77, 1993, pp. 233–262.

[19] M. Nakanishi, K. Tamaki, K. Kobayashi, Magnetic anomaly lineations from late Jurassic to early Cretaceous in the west-central Pacific Ocean, Geophys. J. Int. 109 (1992) 701–719.

[20] M.G. Petterson, C.R. Neal, J.J. Mahoney, L.W. Kroenke, A.D. Saunders, T.L. Babbs, R.A. Duncan, D. Tolia, B. McGrail, Structure and deformation of north and central Malaita, Solomon Islands: tectonic implications for the Ontong Java Plateau-Solomon arc collision, and for the fate of oceanic plateaus, Tectonophysics 283 (1997) 1–33.

[21] H. Mayer, J.A. Tarduno, Paleomagnetic investigation of the igneous sequence, Site 807, Ontong Java plateau, and a discussion of Pacific true polar wander, Proc. ODP Sci. Results 130 (1993) 51–59.

[22] Ö. Özdemir, D.J. Dunlop, An experimental study of chemical remanent magnetizations of synthetic monodomain titanomaghemite with initial thermoremanent magnetizations, J. Geophys. Res. 90 (1985) 11513–11523.
[23] J.L. Kirschvink, The least squares line and plane and the analysis of paleomagnetic data, Geophys. J. R. Astron. Soc. 62 (1980) 699–718.
[24] J.A. Tarduno, R.D. Cottrell, Paleomagnetic evidence for motion of the Hawaiian hotspot during formation of the Emperor seamounts, Earth Planet. Sci. Lett. 153 (1997) 171–180.
[25] M. Antretter, B. Steinberger, F. Heider, H. Soffel, Paleolatitudes of the Kerguelen hotspot: new paleomagnetic results and dynamic modeling, Earth Planet. Sci. Lett. 203 (2002) 635–650.
[26] P.L. McFadden, A.B. Reid, Analysis of paleomagnetic inclination data, Geophys. J. R. Astron. Soc. 69 (1982) 307–319.
[27] L. Tauxe, Paleomagnetic Principles and Practice, Kluwer Academic, 1998, 299 pp.
[28] M. Kono, Paleomagnetism of DSDP Leg 55 basalts and implications for the tectonics of the Pacific plate, DSDP Init. Rep. 55 (1980) 737–752.
[29] T. Pick, L. Tauxe, Geomagnetic palaeointensities during the Cretaceous normal superchron measured using submarine basaltic glass, Nature 366 (1993) 238–242.
[30] S.C. Cande, D.V. Kent, Revized calibration of the geomagnetic polarity timescale for the Late Cretaceous and Cenozoic, J. Geophys. Res. 100 (1995) 6093–6095.
[31] A. Cox, Latitude dependence of the angular dispersion of the geomagnetic field, Geophys. J. R. Astron. Soc. 20 (1970) 253–269.
[32] P.L. McFadden, R.T. Merrill, M.W. McElhinny, S.-h. Lee, Reversals of the Earth's magnetic field and temporal variations of the dynamo family, J. Geophys. Res. 96 (1991) 3923–3933.
[33] J.A. Tarduno, W.W. Sager, Polar standstill of the Mid-Cretaceous Pacific plate and its geodynamic implications, Science 269 (1995) 956–959.
[34] M. Nakanishi, J.S. Gee, Paleomagnetic investigations of volcanic rocks: paleolatitudes of the northwestern Pacific guyots, Proc. ODP Sci. Results 144 (1995) 585–604.
[35] W.W. Sager, A.A.P. Koppers, Late Cretaceous polar wander of the Pacific plate: Evidence of a rapid true polar wander event, Science 287 (2000) 455–459.
[36] K.E. Petronotis, R.G. Gordon, A Maastrichtian palaeomagnetic pole for the Pacific plate from skewness analysis of marine magnetic anomaly 32, Geophys. J. Int. 139 (1999) 227–247.
[37] R.D. Cottrell, J.A. Tarduno, Late Cretaceous true polar wander: Not so fast, Science 288 (2000) 2283a.
[38] S.C. Cande, J.M. Stock, D. Müller, T. Ishihara, Cenozoic motion between East and West Antarctica, Nature 404 (2000) 145–150.
[39] Y.Y. Harada, Y. Hamano, Recent progress on the plate motion relative to hotspots, in: M.A. Richards et al. (Eds.), The History and Dynamics of Global Plate Motions, AGU Monograph 121, 2000, pp. 327–338.
[40] P. Molnar, J. Stock, Relative motions of hotspots in the Pacific, Atlantic and Indian oceans since late Cretaceous time, Nature 327 (1987) 587–591.
[41] J.A. Tarduno, J. Gee, Large-scale motion between Pacific and Atlantic hotspots, Nature 378 (1995) 477–480.
[42] I. Norton, Global hotspot reference frames and plate motion, in: M.A. Richards et al. (Eds.), The History and Dynamics of Global Plate Motions, AGU Monograph 121, 2000, pp. 339–357.
[43] P. Wessel, L. Kroenke, A geometric technique for relocating hotspots and refining absolute plate motions, Nature 387 (1997) 365–369.
[44] A.A.P. Koppers, J.P. Morgan, J.W. Morgan, H. Staudigel, Testing the fixed hotspot hypothesis using Ar-40/Ar-39 age progressions along seamount trails, Earth Planet. Sci. Lett. 185 (2001) 237–252.
[45] D.C. Engebretson, A. Cox, R.G. Gordon, Relative motions between oceanic and continental plates in the Pacific Basin, Geol. Soc. Am. Spec. Paper 206, 1985.
[46] P. Lonsdale, Geography and history of the Louisville hotspot chain in the southwest Pacific, J. Geophys. Res. 93 (1988) 3078–3104.
[47] R. Van der Voo, T.H. Torsvik, Evidence for late Paleozoic and Mesozoic non-dipole fields provides and explanation for the Pangea reconstruction problems, Earth Planet. Sci. Lett. 187 (2001) 71–81.
[48] D.T. Sandwell, W.H.F. Smith, Marine gravity anomaly from Geosat and ERS-1 satellite altimetry, J. Geophys. Res. 102 (1997) 10039–10054.
[49] G.A. Acton, R.G. Gordon, A 65 Ma paleomagnetic pole for the Pacific plate from the skewness of magnetic anomlies 27r-31, Geophys. J. Int. 106 (1991) 407–420.
[50] K.E. Petronotis, R.G. Gordon, G.D. Acton, A 57 Ma Pacific plate paleomagnetic pole determined from a skewness analysis of crossings of marine magnetic anomaly 25r, Geophys. J. Int. 118 (1994) 529–554.
[51] K.E. Petronotis, R.G. Gordon, G.D. Acton, Determining palaeomagnetic poles and anomalous skewness from marine magnetic anomaly skewness data from a single plate, Geophys. J. Int. 109 (1992) 209–224.